university of groningen

University Medical Center Groningen

University of Groningen

24-mu m spin relaxation length in boron nitride encapsulated bilayer graphene

Ingla Aynés, Josep; Guimaraes, M. H. D.; Meijerink, R. J.; Zomer, P. J.; van Wees, Bart

Published in:
Physical Review. B: Condensed Matter and Materials Physics

DOI:
10.1103/PhysRevB.92.201410

IMPORTANT NOTE: You are advised to consult the publisher's version (publisher's PDF) if you wish to cite from it. Please check the document version below.

Document Version
Publisher's PDF, also known as Version of record

Publication date:
2015

Link to publication in University of Groningen/UMCG research database

Citation for published version (APA):
Ingla-Aynes, J., Guimaraes, M. H. D., Meijerink, R. J., Zomer, P. J., & van Wees, B. J. (2015). 24-mu m spin relaxation length in boron nitride encapsulated bilayer graphene. Physical Review. B: Condensed Matter and Materials Physics, 92(20), [201410]. DOI: 10.1103/PhysRevB.92.201410

Copyright
Other than for strictly personal use, it is not permitted to download or to forward/distribute the text or part of it without the consent of the author(s) and/or copyright holder(s), unless the work is under an open content license (like Creative Commons).

Take-down policy
If you believe that this document breaches copyright please contact us providing details, and we will remove access to the work immediately and investigate your claim.

Downloaded from the University of Groningen/UMCG research database (Pure): http://www.rug.nl/research/portal. For technical reasons the number of authors shown on this cover page is limited to 10 maximum.

Download date: 11-02-2018

PHYSICAL REVIEW B **92**, 201410(R) (2015)

24-μm spin relaxation length in boron nitride encapsulated bilayer graphene

J. Ingla-Aynés,[1,*] M. H. D. Guimarães,[1,2] R. J. Meijerink,[1] P. J. Zomer,[1] and B. J. van Wees[1]
[1]*Physics of Nanodevices, Zernike Institute for Advanced Materials, University of Groningen, The Netherlands*
[2]*Kavli Institute at Cornell, Cornell University, Ithaca, New York 14853, USA*

(Received 1 June 2015; revised manuscript received 28 August 2015; published 19 November 2015)

We have performed spin and charge transport measurements in dual gated high mobility bilayer graphene encapsulated in hexagonal boron nitride. Our results show spin relaxation lengths λ_s up to 13 μm at room temperature with relaxation times τ_s of 2.5 ns. At 4 K, the diffusion coefficient rises up to 0.52 m^2/s, a value five times higher than the best achieved for graphene spin valves up to date. As a consequence, λ_s rises up to 24 μm with τ_s as high as 2.9 ns. We characterized three different samples and observed that the spin relaxation times increase with the device length. We explain our results using a model that accounts for the spin relaxation induced by the nonencapsulated outer regions.

DOI: 10.1103/PhysRevB.92.201410 PACS number(s): 72.80.Vp, 72.25.−b, 85.75.Hh

Graphene and its multilayer forms are ideal platforms to transport spin information. Theoretical predictions suggest that spin relaxation times (τ_s) up to 100 ns can be achieved in single layer pristine graphene [1] and the experimental results for graphene on SiO_2 showed $\tau_s \approx 150$ ps [2].

In this context, experiments focused on the spin transport properties of bilayer graphene [3,4] reported nanosecond spin relaxation times. The inverse relation obtained between τ_s and the diffusion coefficient (D) suggested that the D'yakonov-Perel [5] mechanism dominates spin relaxation in bilayers. However, in single layers, the observed linear dependence suggested that the Elliot-Yafet [6] mechanism may dominate the spin relaxation [3]. These results triggered the discussion about the differences between both systems.

Recent theoretical works on spin relaxation in single [7,8] and bilayer [9] graphene provided models that give relaxation rates in the order of the experimental ones. These models also predict different τ_s-D dependencies compared with the ones expected from the abovementioned mechanisms [10].

Recent experiments which used hexagonal boron nitride (BN) to encapsulate single layer graphene achieved spin relaxation times up to 2 ns at room temperature in high mobility devices. Such devices showed record relaxation lengths up to 12 μm [11]. Other results on partially suspended multilayer graphene covered by BN achieved room temperature τ_s up to 3.9 ns in trilayer graphene [12], showing the potential of graphene/BN heterostructures for spin transport.

In this Rapid Communication we report spin transport in high mobility bilayer graphene (BLG). Our samples consist of BLG that is partially encapsulated between two BN flakes and fabricated as in [11]. Fabrication details can be found in the Supplemental Material [13]. The sample configuration is shown in the inset of Fig. 1. The bilayer graphene, in black, is encapsulated between the top and bottom BN. The flake is fully encapsulated in the central region while both left and right sides are not encapsulated but only supported on a bottom BN. This configuration allows us to have ferromagnetic contacts at both sides of the sample while keeping the central region protected.

The top gate together with the Si back gate [Fig. 1(b) inset], allow us to simultaneously control the electric field $\overline{E} = (V_{bg} - V_{bg}^{(0)})/2d_{bg} - (V_{tg} - V_{tg}^{(0)})/2d_{tg}$ and the carrier density $n = \epsilon_0\epsilon_{bg}(V_{bg} - V_{bg}^{(0)})/ed_{bg} + \epsilon_0\epsilon_{tg}(V_{tg} - V_{tg}^{(0)})/ed_{tg}$ applied to the dual-gated region. Here e is the electron charge, ϵ_0 is the vacuum permittivity, $\epsilon_{bg(tg)} \approx 3.9$ is the dielectric permittivity, $d_{bg(tg)}$ is the thickness of the dielectric, $V_{bg(tg)}$ is the applied gate voltage, and $V_{bg(tg)}^{(0)}$ is the voltage at the charge neutrality point of the back gate (top gate), respectively [14].

We have characterized three devices (A, B, and C) showing similar results at room temperature and 4 K. The results are shown in Table I. From there we can see that τ_s seems to depend on the length of the encapsulated region and, even though device C shows a higher spin diffusion coefficient (D_s) than device B, indicating better electronic quality, τ_s of device B is more than two times longer than the one of device C. This nonstraightforward connection between electronic quality and τ_s seems to be in agreement with the results shown in [15] for single layer graphene, while the length dependence can be explained by the effect of the invasive contacts and the lower quality of the nonencapsulated regions being reduced increasing the contact separation [16,17].

From now on we will discuss the results obtained at 4 K for device A. The contact resistances range between 280 Ω and 2.7 kΩ. These low values are a consequence of imperfect tunnel barriers and affect the spin transport measurements [16].

In Fig. 1(a) we show the square resistance (R_{sq}) of the encapsulated region as a function of the back-gate voltage (V_{bg}) and the top-gate voltage (V_{tg}). The charge neutrality point appears as a line with a slope $-C_{bg}/C_{tg} = -0.078$ showing a resistance minimum at $V_{bg} = -8$ V, $V_{tg} = -0.7$ V. Taking into account that this point has zero carrier density and zero electric field we can estimate the doping at the top and bottom sides of the flake: $n_{bg}^{(0)} \approx n_{tg}^{(0)} \approx 5.5 \times 10^{15}$ m^{-2}.

The resistance increases at both sides of the charge neutrality line, reaching up to 38 kΩ at an electric field of 0.2 V/nm. This is caused by the opening of a gap driven by the electric field [14]. One can also distinguish two V_{tg} independent features coming from the non-top-gated region between the inner contacts. One comes from the sides of the encapsulated regions that are non-top-gated and show a charge neutrality point around $V_{bg} = -19$ V. The other comes from

*j.ingla.aynes@rug.nl

 ©2015 American Physical Society

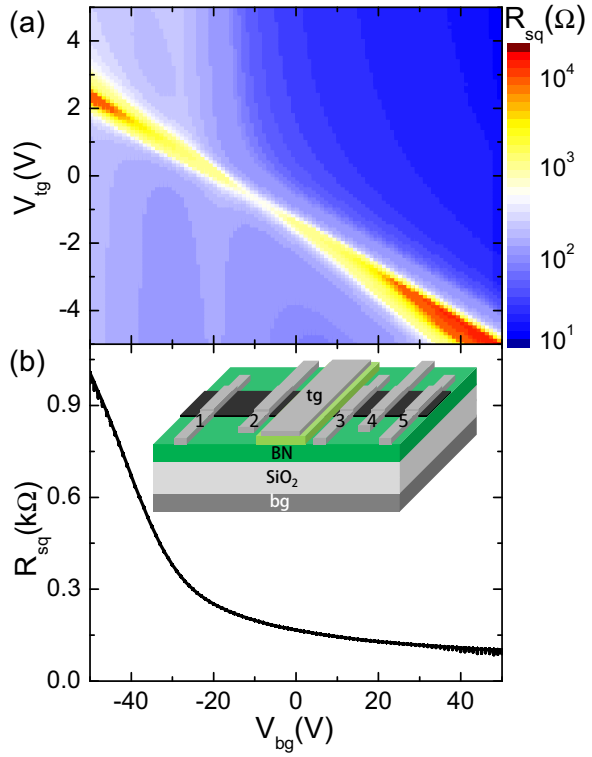

FIG. 1. (Color online) (a) Square resistance obtained between contacts 2 and 3 (in color scale) with respect to V_{tg} (y axis) and V_{bg} (x axis) (b) Square resistance of the nonencapsulated region measured between contacts 3 and 4. Inset: Schematics of the device.

the nonencapsulated regions and its square resistance is shown in Fig. 1(b).

The mobility (μ) obtained for this sample at $V_{bg} = -8$ V (zero electric field) is 16 m^2/V s at the electron side. The value is obtained using the formula $R_{sq} = 1/ne\mu + \rho_s$, where $\rho_s \approx 57\ \Omega$ is the n-independent resistivity component coming from the effect of the resistance of the non-top-gated regions between the inner contacts and short-range scattering [18]. We have also confirmed that the resistance of the outer regions of the sample does not depend on V_{tg}.

In Fig. 1(b) we show the V_{bg} dependence of one of the outer regions' resistance. As it can be seen from the graph, the charge neutrality point is below $V_{bg} = -50$ V and falls outside our gate range. We attribute this to the contamination given by the polymers used during fabrication.

TABLE I. Spin parameters obtained at the gate combination giving the longest λ_s for three devices with different lengths of the encapsulated regions. L_{enc} is the length of the encapsulated region and d_{2-3} is the separation between the inner contacts.

Dev.	L_{enc} (μm)	d_{2-3} (μm)	T (K)	τ_s (ns)	D_s (m^2/s)	λ_s (μm)
A	13.2	14.6	300	2.5	0.07	13
			4	2.9	0.2	24
B	8.5	10.3	300	1.1	0.03	5.7
			4	1.9	0.05	9.7
C	6.2	7.8	300	0.32	0.04	3.6
			4	0.45	0.07	5.6

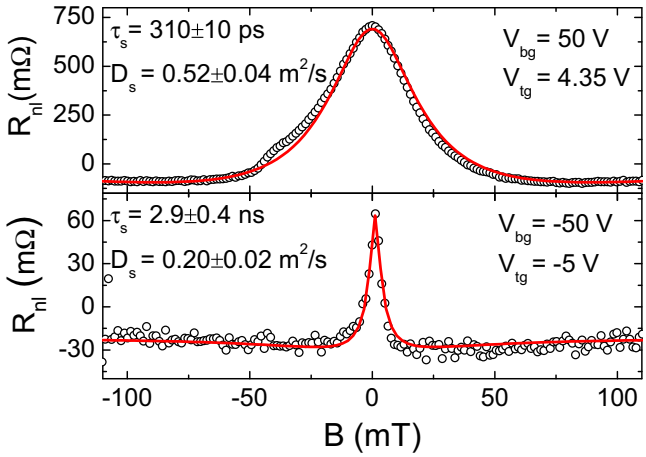

FIG. 2. (Color online) Hanle precession curves obtained at 4 K for $V_{bg} = -50$ V, $V_{tg} = -5$ V (top panel) and $V_{bg} = 50$ V, $V_{tg} = 4.35$ V (bottom panel) with the corresponding fitting curves and extracted spin parameters.

To measure the spin transport properties of the encapsulated region, we used the standard nonlocal geometry [19]. When applying an out-of-plane magnetic field the spins undergo Larmor precession. Measuring $R_{nl} = V_{3-5}/I_{1-2}$ while sweeping the magnetic field we obtained the so called Hanle precession curves. To eliminate spin-independent effects we have taken Hanle curves for parallel and antiparallel magnetic configurations of the inner contacts and subtracted them $R_{nl} = (R_{nl}^{par} - R_{nl}^{anti})/2$, where $R_{nl}^{par(anti)}$ is the nonlocal resistance in the parallel (antiparallel) magnetic configuration [16]. The magnetizations of the contacts are tuned applying an in-plane magnetic field.

In Fig. 2 we show two Hanle curves taken at $V_{bg} = 50$ V, $V_{tg} = 4.35$ V and $V_{bg} = -50$ V, $V_{tg} = -5$ V, corresponding to the top right and bottom left corners in the color plot of Fig. 1(a). The spin relaxation time and diffusion coefficients are extracted from these curves by fitting them with the solution of the Bloch equations [5,19] including a small offset [20].

The spin signal at $V_{bg} = 50$ V, $V_{tg} = 4.35$ V (Fig. 2 top panel) is 10 times higher than the one at $V_{bg} = -50$ V, $V_{tg} = -5$ V (Fig. 2 bottom panel). This is most likely due to the low resistance of our contacts. At $V_{bg} = -50$ V the contact resistance is in the order of the spin resistance of the channel ($R_\lambda = R_{sq}\lambda_s/W$, here W is the width of the sample), part of the injected spin accumulation relaxes back to the contacts instead of diffusing in the channel, reducing the effective injection efficiency [16,21] from 12% to 2%. This effect is mainly ruled by the resistance of the outer regions (where the contacts are placed) and may also be amplified by the presence of pn junctions at $V_{bg} = -50$ V, $V_{tg} = -5$ V.

In Fig. 3(a) we show the spin diffusion coefficient as a function of the top-gate voltage for three different back-gate voltages. The charge diffusion coefficients (D_c solid lines) are extracted using the Einstein relation $1/D_c = e^2 R_{sq} \nu(E_F)$, where $\nu(E_F)$ is the density of states at the Fermi energy and e is the electron charge. R_{sq} was taken from Fig. 1(a) and corrected by subtracting the resistance of the nonencapsulated regions between the inner contacts.

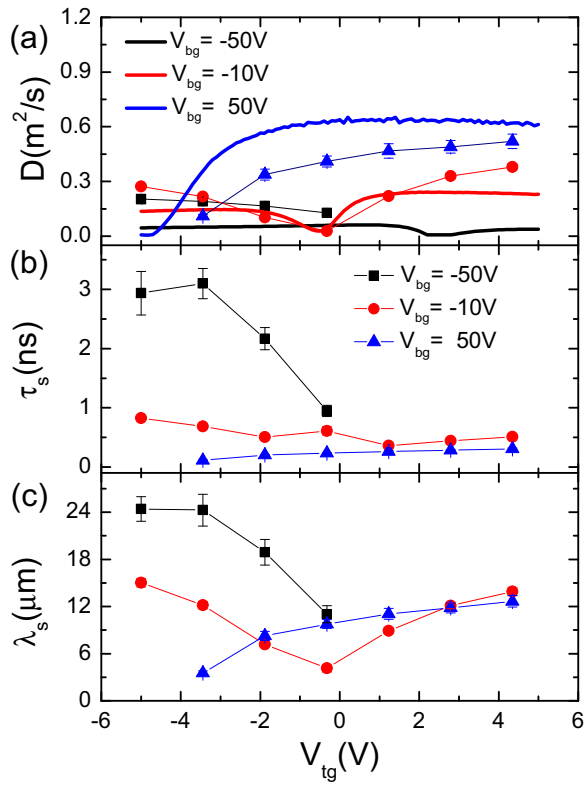

FIG. 3. (Color online) Spin transport parameters obtained by fitting the Hanle curves at 4 K as a function of V_{tg} for $V_{bg} = -50$, -10, and 50 V. (a) Spin diffusion coefficient (dots) compared with the charge diffusion coefficient (solid lines), (b) spin relaxation time, and (c) the relaxation length. The lines connecting the spin parameters are a guide to the eye.

At $V_{bg} = -50$ V one can observe a substantial difference between D_c and D_s. We attribute this to the fact that the gate induced doping of the encapsulated and nonencapsulated regions have different signs, creating *pn* junctions of unknown widths at the boundaries. Since these boundaries are between the inner contacts, the measured square resistances are no longer characteristic of the channel itself but of the junctions. This affects the determination of D_c.

At $V_{bg} = 50$ V both encapsulated and nonencapsulated regions are electron doped and D_c shows better agreement with respect to D_s, supporting the validity of the parameters obtained from the Hanle measurements. The minor discrepancy in this case can be attributed to the small resistance of the encapsulated non-top-gated region that was not subtracted from the calculation of R_{sq}. D_c and D_s reach values above 0.5 m^2/s, five times higher than the best achieved for BN encapsulated single layer graphene spin valve devices [11].

At $V_{bg} = -10$ V (approximately zero electric field) we see that close to the charge neutrality point ($V_{tg} \approx 0$ V) there is a better agreement between D_c and D_s than at high carrier densities. This can be explained taking into account that close to the charge neutrality point the square resistance of the encapsulated region is high enough to dominate the measurement of R_{sq}, but at high carrier densities the square resistance of the encapsulated region is small and the contributions of the non-top-gated regions become relevant.

In Fig. 3(b) there is a strong dependence of τ_s on V_{bg}. At $V_{bg} = -50$ V the relaxation time reaches 2.9 ns, while at 50 V a maximum of $\tau_s = 310$ ps is obtained. This reduction of a factor 10 in τ_s is in agreement with the results in [11] and can be explained as an effect of the change in R_λ of the nonencapsulated regions. As the spin resistance of these regions increases, their influence on the spin relaxation is reduced. This effect occurs because the spins relax predominantly at the regions with the lower R_λ.

The opposite effect occurs when opening a gap in the encapsulated region and its square resistance increases with respect to the one of the nonencapsulated part. Since τ_s is longer in the encapsulated region than in the outer ones, R_λ gets orders of magnitude higher than the one of the outer part. As a consequence, the spin relaxation is dominated by the nonencapsulated regions and the amplitude of the spin signal vanishes. This effect explains why we could not measure spin signals at $V_{bg} = -50$ V and positive V_{tg}.

In Fig. 3(c) we show the spin relaxation lengths calculated using the formula $\lambda_s = \sqrt{D_s \tau_s}$. λ_s goes up to 24 μm, the highest value achieved up to date by fitting Hanle measurements in nonlocal geometry. Note that, even though spin relaxation lengths up to 280 μm were estimated from local two probe measurements at 4 K for epitaxial graphene on a SiC substrate [22], no Hanle measurements were done to support these values.

Since the spins probe the whole device (inner and outer regions), we have to account for the nonhomogeneity of our sample to explain our results. For this reason we use the same model as in [11] and [23], where we solve the Bloch equations for a nonhomogeneous system consisting of a central region sandwiched by two regions as shown in the inset of Fig. 4. We set the spin and charge transport parameters (τ_s, D_s, and R_{sq}) for the three regions assuming that the outer regions are identical. After simulating the corresponding Hanle curves, we fit them using a homogeneous model as we have done with our experimental data. From this procedure we obtain the effective relaxation time of the system (τ_{eff}).

The effect of invasive contacts is taken into account using the spin transport parameters obtained from Hanle measurements carried out at the nonencapsulated regions. Since the contact separation in these regions is between 1 and 2 μm, the extracted parameters are strongly affected by the low contact resistances [16].

In Fig. 4 we plot τ_{eff} as a function of the spin relaxation time in the encapsulated region (τ_{enc}) for three different values for the spin relaxation time in the nonencapsulated region (τ_{non}). The resistance values used for the central region are the ones used to calculate D_c in Fig. 3(a). For the diffusion coefficient in the encapsulated region (D_{enc}) we have used the values of D_s extracted from the experiments at the encapsulated region. This is justified since D_s is not affected by the outer regions [11,23]. The square resistance of the nonencapsulated region is taken from Fig. 1(b) and the diffusion coefficient (D_{non}) is taken from the experimental Hanle curves obtained at the outer region.

In Fig. 4(a), where $V_{bg} = -50$ V and $V_{tg} = -5$ V, the maximum τ_{eff} obtained from the simulations reaches 1.8 ns for $\tau_{enc} = 100$ ns and $\tau_{non} = 300$ ps. This value is still below the 2.9 ns obtained from the fittings of the encapsulated data. This discrepancy can be explained taking into account that we

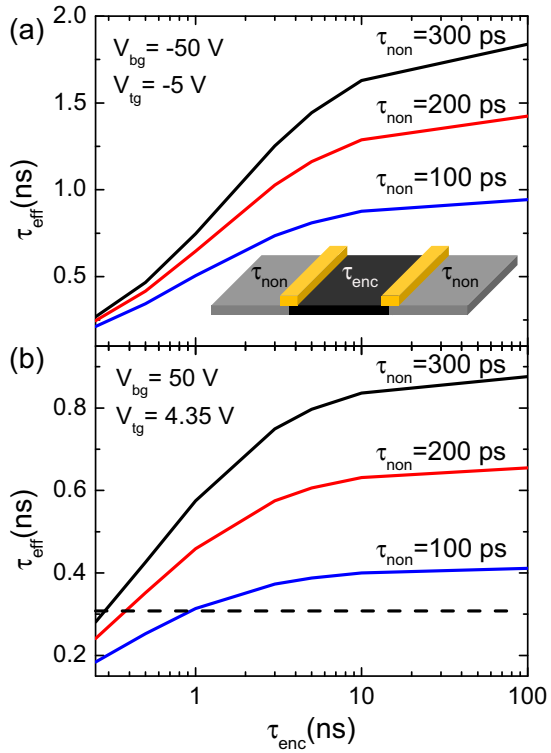

FIG. 4. (Color online) Effective spin relaxation time in the system as a function of τ_{enc} for three different values of τ_{non} at $V_{bg} = -50$ V and $V_{tg} = -5$ V (a) and $V_{bg} = 50$ V and $V_{tg} = 4.35$ V (b), the dashed line is the experimental value of τ_{eff}, taken from Fig. 2 (top panel). The inset shows a cartoon device of the simulated system.

have an *npn* system and there are high resistive *pn* junctions that may affect the spin diffusion between the encapsulated and nonencapsulated regions. This is not taken into account in our simulations.

The simulations at $V_{bg} = 50$ V and $V_{tg} = 4.35$ V are shown in Fig. 4(b). Here both encapsulated and nonencapsulated regions are *n* doped and there are no *pn* junctions. The dashed line at 310 ps corresponds to the value obtained from the fittings of the experimental results at the encapsulated region. The intersections between the simulated curves and the dashed line give us the possible values of τ_{enc}. From the fittings of the Hanle curves measured at the outside regions, we obtained $\tau_{non} \approx 100$ ps. As a consequence, from our simulations, τ_{enc} is of the order of 1 ns. Using this relaxation time and $D_{enc} = 0.52$ m^2/s, we can calculate the spin relaxation length of the encapsulated region. It is 22 μm, close to the 24 μm, suggesting that most of the spin relaxation takes place at the nonencapsulated regions.

In conclusion, we have characterized three boron nitride encapsulated bilayer graphene devices with 13.2-, 8.5-, and 6.2-μm-long encapsulated regions showing consistent behavior where τ_s depends on the length of the encapsulated region.

The results obtained for the longer device show unprecedented large spin diffusion coefficients up to 0.52 m^2/s at 4 K, five times higher than the best achieved for single layer graphene using the same geometry [11]. As a consequence, the spin relaxation length rises up to 13 μm at room temperature and 24 μm at 4 K.

Our simulations using a three regions model show that the measured spin relaxation times of 2.5 ns at room temperature and 2.9 ns at 4 K are most likely limited by the outer regions, suggesting that it is possible to transport spin information over even larger distances in the used geometry by increasing the length of the encapsulated region. According to this result, higher spin relaxation times can be achieved by making longer devices [17].

We would like to acknowledge J. C. Brant, R. Ruiter, and J. C. Leutenantsmeyer for useful discussions and J. G. Holstein, H. M. de Roosz, H. Adema, and T. Schouten for technical support. The research leading to these results has received funding from the People Programme (Marie Curie Actions) of the European Union's Seventh Framework Programme FP7/2007-2013/ under REA grant agreement No. 607904-13 Spinograph, the Dutch Foundation for Fundamental Research on Matter (FOM), the European Union Seventh Framework Programme under grant agreement No. 604391 Graphene Flagship, the Netherlands Organization for Scientific Research (NWO), NanoNed, and the Zernike Institute for Advanced Materials.

[1] D. Huertas-Hernando, F. Guinea, and A. Brataas, Phys. Rev. Lett. **103**, 146801 (2009).
[2] N. Tombros, C. Jozsa, M. Popinciuc, H. T. Jonkman, and B. J. van Wees, Nature (London) **448**, 571 (2007).
[3] W. Han and R. K. Kawakami, Phys. Rev. Lett. **107**, 047207 (2011).
[4] T.-Y. Yang, J. Balakrishnan, F. Volmer, A. Avsar, M. Jaiswal, J. Samm, S. R. Ali, A. Pachoud, M. Zeng, M. Popinciuc, G. Güntherodt, B. Beschoten, and B. Özyilmaz, Phys. Rev. Lett. **107**, 047206 (2011).
[5] J. Fabian, A. Matos-Abiague, C. Ertler, P. Stano, and I. Zutic, Acta. Phys. Slovaca **57**, 565 (2007).
[6] H. Ochoa, A. H. Castro Neto, and F. Guinea, Phys. Rev. Lett. **108**, 206808 (2012).
[7] D. Kochan, M. Gmitra, and J. Fabian, Phys. Rev. Lett. **112**, 116602 (2014).
[8] D. Van Tuan, F. Ortmann, D. Soriano, S. O. Valenzuela, and S. Roche, Nat. Phys. **10**, 857 (2014).
[9] D. Kochan, S. Irmer, M. Gmitra, and J. Fabian, Phys. Rev. Lett. **115**, 196601 (2015).
[10] Y. Song and H. Dery, Phys. Rev. Lett. **111**, 026601 (2013).
[11] M. H. D. Guimarães, P. J. Zomer, J. Ingla-Aynés, J. C. Brant, N. Tombros, and B. J. van Wees, Phys. Rev. Lett. **113**, 086602 (2014).

[12] M. Drögeler, F. Volmer, M. Wolter, B. Terrs, K. Watanabe, T. Taniguchi, G. Gntherodt, C. Stampfer, and B. Beschoten, Nano Lett. **14**, 6050 (2014).

[13] See Supplemental Material at http://link.aps.org/supplemental/10.1103/PhysRevB.92.201410 for detailed description of the device fabrication, transport measurements, determination of the mobility of the sample and room temperature results for device A.

[14] Y. Zhang, T. Tang, C. Girit, Z. Hao, M. C. Martin, A. Zettl, M. F. Crommie, Y. R. Shen, and F. Wang, Nature (London) **459**, 820 (2009).

[15] W. Han, J.-R. Chen, D. Wang, K. M. McCreary, H. Wen, A. G. Swartz, J. Shi, and R. K. Kawakami, Nano Lett. **12**, 3443 (2012).

[16] T. Maassen, I. J. Vera-Marun, M. H. D. Guimarães, and B. J. van Wees, Phys. Rev. B **86**, 235408 (2012).

[17] M. V. Kamalakar, C. Groenveld, A. Dankert, and S. P. Dash, Nat. Commun. **6**, 6766 (2015).

[18] S. V. Morozov, K. S. Novoselov, M. I. Katsnelson, F. Schedin, D. C. Elias, J. A. Jaszczak, and A. K. Geim, Phys. Rev. Lett. **100**, 016602 (2008).

[19] M. Johnson and R. H. Silsbee, Phys. Rev. B **37**, 5312 (1988).

[20] F. Volmer, M. Drögeler, T. Pohlmann, G. Güntherodt, C. Stampfer, and B. Beschoten, 2D Mater. **2**, 024001 (2015).

[21] F. Volmer, M. Drögeler, E. Maynicke, N. von den Driesch, M. L. Boschen, G. Güntherodt, C. Stampfer, and B. Beschoten, Phys. Rev. B **90**, 165403 (2014).

[22] B. Dlubak, M.-B. Martin, C. Deranlot, B. Servet, S. Xavier, R. Mattana, M. Sprinkle, C. Berger, W. A. De Heer, F. Petroff, A. Anane, P. Seneor, and A. Fert, Nat. Phys. **8**, 557 (2012).

[23] M. H. D. Guimarães, A. Veligura, P. J. Zomer, T. Maassen, I. J. Vera-Marun, N. Tombros, and B. J. van Wees, Nano Lett. **12**, 3512 (2012).